Physics of Plasmas

Boundary-induced effect on the spoke-like activity in $E \times B$ plasma

Cite as: Phys. Plasmas **26**, 053503 (2019); https://doi.org/10.1063/1.5092702
Submitted: 13 February 2019 . Accepted: 10 April 2019 . Published Online: 07 May 2019

E. Rodríguez, V. Skoutnev, Y. Raitses, A. Powis, I. Kaganovich, and A. Smolyakov

Physics of Plasmas ARTICLE scitation.org/journal/php

Boundary-induced effect on the spoke-like activity in $E \times B$ plasma

Cite as: Phys. Plasmas **26**, 053503 (2019); doi: 10.1063/1.5092702
Submitted: 13 February 2019 · Accepted: 10 April 2019 ·
Published Online: 7 May 2019

E. Rodríguez,[1,a)] V. Skoutnev,[1] Y. Raitses,[1,b)] A. Powis,[1] I. Kaganovich,[1] and A. Smolyakov[2]

AFFILIATIONS

[1]Princeton Plasma Physics Laboratory, Princeton, New Jersey 08540, USA
[2]University of Saskachewan, Saskatoon, Saskatchewan S7N 5E2, Canada

[a)]eduardor@princeton.edu
[b)]yraitses@pppl.gov

ABSTRACT

The spoke instability in an $E \times B$ Penning discharge is shown to be strongly affected by the boundary that is perpendicular to B field lines. The instability is the strongest when bounded by dielectric walls. With a conducting wall, biased to collect electron current from the plasma, the spoke becomes faster, less coherent, and localized closer to the axis. The corresponding anomalous cross-field transport is assessed via simultaneous time-resolved measurements of plasma potential and density. This shows a dominant large-scale $E \times B$ anomalous character of the electron cross-field current for dielectric walls reaching 40%–100% of the discharge current, with an effective Hall parameter $\beta_{\text{eff}} \sim 10$. The anomalous current is greatly reduced with the conducting boundary (characterized by $\beta_{\text{eff}} \sim 10^2$). These experimental measurements are shown to be qualitatively consistent with the decrease in the E field that triggers the collisionless Simon-Hoh instability.

I. INTRODUCTION

Cross-field discharges such as Hall thrusters[1–3] for space applications[4] and sputtering magnetrons[5,6] for material processing[7] are susceptible to a number of performance-limiting unstable mechanisms.[8–10] A better understanding of their physical origin thus proves essential.

Especially relevant, and the subject that is to concern us here, is the so-called "spoke"[11–15] (see Fig. 1). This azimuthally rotating macroscopic structure of increased plasma density and enhanced ionization is common to many $E \times B$ devices. Its rotation occurs quasi-coherently in the $E \times B$ direction, but with a speed slower than the $E \times B$ drift of magnetized electrons (typically by an order of magnitude). Moreover, the presence of the spoke has been associated in the literature with an increase in the electron cross-field mobility.[13,16–19] This enhanced transport is significantly larger than those values expected from classical collisional calculations and in this sense is deemed anomalous. This current has deleterious effects in, for example, Hall thrusters[20] and is therefore a feature sought to be understood, controlled, and ultimately eliminated.

In the sake of understanding the origin of the spoke, many phenomenological accounts of potential sources, such as propagating ionization fronts,[17] have been proposed. Studies of linear instabilities have also been carried out, leading to possible numerous growing modes.[21–25] Among these, the Simon-Hoh instability,[26,27] originating from colinear E field and density gradients, has drawn renewed attention. In particular, its collisionless version[25] is driven exclusively by the electron $E \times B$ drift, and more complete considerations have also been recently proposed as part of general theory of gradient drift instabilities (GDIs).[24,28–30]

Alongside these theoretical efforts, computational modeling has become increasingly important in extending the present understanding of the spoke. Among the many numerical approaches available,[31–34] simulations employing Particle-in-cell (PIC) codes[33,35] have lately gained relevance, including simulations of real sized devices.[36] Indeed, "spoke-like" structures have been shown to appear in such recreated devices even in the simplest formulations, such as in the absence of ionization or collisions.[33,36]

Imperative to the validity of all these existing predictions is, however, empirical evidence. This paper presents the results of experimental studies of the $E \times B$ discharge shown in Fig. 2 with a focus on the effects that changing boundary conditions have on the spoke activity. In particular, we show that the shortening of the $E \times B$ plasma by a metal wall as facing flange (see Fig. 2) significantly reduces the spoke activity in part due to the reduction of the electric field but does not suppress it completely. The shortening of the $E \times B$ plasma with the conductive wall is similar to the well-known Simon's effect,[37] but its effect on the spoke is the finding of this paper. Indeed, a different type

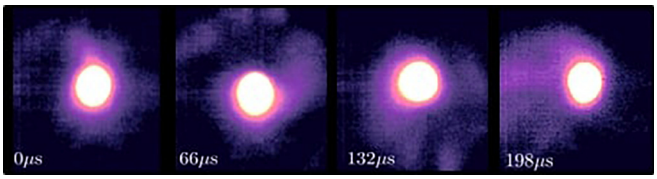

FIG. 1. Rotating spoke seen along the axis of the Penning device with a fast-frame camera. $B = 80$ G is out of the page and E is radially inward (Xenon at 0.2 mTorr pressure).

of azimuthal activity with twice and three times higher frequencies than typical spoke oscillations and modified spatial distribution is observed for the same operating conditions as in the $E \times B$ plasma bounded with dielectric walls as facing flange. An enhanced cross-field electron conduction due to perturbations by the spoke is also studied and significantly reduced. A final comparison to some predictions of the collisionless Simon-Hoh instability (CSHI) is also presented.

II. EXPERIMENTAL BACKGROUND

A. Theoretical basis

For an analysis of experimental results and their comparison with theoretical predictions, collisionless Simon-Hoh instability (CSHI) is considered here, as developed originally in Ref. 25 and obtained as a limiting form of GDI in Refs. 28 and 29.

The classical CSHI theory invokes the following assumptions. First of all, the approach is linear and is developed for an infinite slab geometry, with one periodic coordinate and a uniform direction. Second, both electrons and ions are treated as collisionless fluids but, the plasma is only partially magnetized. Then, magnetized electrons have significant $E \times B$ and diamagnetic drifts. Finally, and particular to the Penning discharge, the magnetic field gradients are neglected in comparison to potential or density ones.

This fluid mode is dominated by the radial electric field, E_r, and density gradient length scale, $L_n^{-1} \equiv |\nabla n|/n$. The form of the dispersion is given by[25]

$$\frac{\omega_*}{\omega - \omega_0} = \frac{k_\theta^2 c_s^2}{\omega^2}, \tag{1}$$

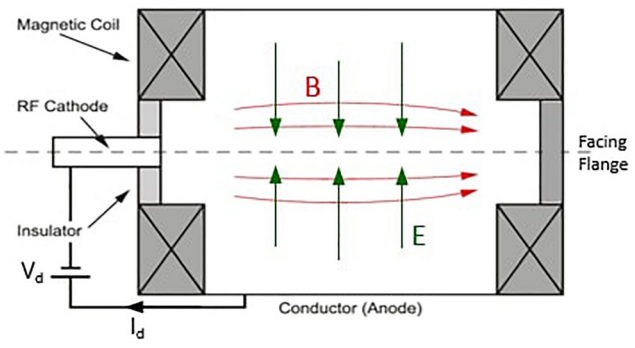

FIG. 2. Diagram showing a longitudinal cut of the Penning device including main features.

where $\omega_* = -k_\theta k_B T_e/eBL_n$ is the electron diamagnetic drift frequency, $\omega_0 = k_\theta E_r/B$ is the $E \times B$ drift frequency, c_s is the ion sound speed, and k_θ is the azimuthal wavenumber.

From Eq. (1), the growth rate γ of the instability is

$$\gamma = \frac{k_\theta c_s}{\omega_*}\sqrt{\omega_0\omega_* - \frac{k_\theta^2 c_s^2}{4}}. \tag{2}$$

It is readily seen that for the system to be unstable (i.e., γ real), collinearity of E_r and the density gradients is necessary, as it is the case in these experiments (see Appendix B).

B. Experimental setup

The entirety of the experiments presented in this paper was done in the $E \times B$ Penning setup shown in Fig. 2 and described elsewhere.[38] The simplicity of this experiment makes it an attractive case of study, still bearing common ground with other larger efforts with similar geometry such as, for example, MISTRAL[39] and LAPD.[40]

In this setup, a partially magnetized plasma with an electron temperature and a density of $T_e \sim 1$–5 eV and $n \sim 10^{16}$–10^{17} m^{-3}, respectively, is generated in a 26 cm diameter (D) and 50 cm length (L) nonmagnetic, stainless steel, 6-way cross chamber equipped with a turbomolecular pump and a mechanical pump. Xenon is employed as the working gas, at a relatively low operating pressure of 0.2 mTorr.

The plasma in the chamber is generated by impact ionization of Xenon atoms with energetic electrons extracted from the RF-plasma cathode.[41] These energetic electrons are extracted applying a voltage of $V_d \sim 55$ V between a metal wall in the RF cathode itself and the chamber (ground). Thus, the chamber acts as the electron collecting anode. The extracted electrons are injected into the chamber along a solenoidal-type magnetic field of $B = 30$–150 G produced by a set of coils placed outside the chamber, strong enough to magnetize electrons. Indeed, under typical operating conditions, the electron gyroradius is $\rho_e \sim 0.3 - 1.7$ mm $\ll D, L$, while ions are on average weakly to nonmagnetized ($\rho_i \sim$0.3–1.5 m). A radial E field is also present, with magnitudes $E \lesssim 200$ Vm^{-1}. In the described experiments, the extraction current (equal to the DC discharge current) was limited to $I_d \sim 1.2$ A.

In order to study the effect of boundary conditions on the spoke and the electron cross-field current, the Penning setup was operated in two configurations. In one configuration (case I), the chamber walls perpendicular to the magnetic field lines (see facing flange in Fig. 2) were dielectric, made from either machinable glass ceramic or Pyrex. The transparent Pyrex was used to allow monitoring the spoke activity with a fast framing camera (see Fig. 1). There were no observable differences in the plasma operation of the Penning discharge between these two dielectric materials.

In the other configuration of the Penning discharge (case II), a nonmagnetic stainless steel flange was used as a magnetic field facing wall. The wall was electrically connected to the chamber and, thereby, it also acted as the anode with respect to the RF cathode. In this setup, the electron flow from the cathode is anticipated to be directly collected along the magnetic field lines connecting the cathode and the flange (Fig. 2).[37] It is also expected that, under such conditions, the plasma confined within the flux tube connecting the cathode and the anode will be close to equipotentiality. Then, in the absence of the electric field across the magnetic field, Eq. (2) predicts no CSHI instability.

In this context, a reduced spoke activity would be consistent with CSHI and could be taken as an indication that CSHI likely plays a role in the spoke formation. The purpose of experiments in this Penning discharge configuration is, in part, to test this prediction.

C. Plasma diagnostics

1. Plasma density (n): Ion probes

A negatively biased ion probe is used to deduce plasma density, n. The probe collects saturated current, I_{ion}, in the Bohm regime,[42] without significant sheath expansion. The lack of expansion was experimentally resolved by observing collection current variations when changing probe negative bias; this gave changes below 5% per 10 V. A 10 kΩ shunt resistor was used to measure the current in the probe circuit. Thus, from the voltage drop measured across the shunt, the ion density is given as

$$n = \frac{I_{\text{ion}}}{\Gamma e A_p c_s}, \tag{3}$$

where $c_s = \sqrt{k_B T_e / M}$ is the Bohm velocity and A_p is the probe area.

The factor Γ corresponds to a geometry dependent, effective pre-sheath density correction from radial motion limited theory.[43] A constant approximated value of $\Gamma \sim 1$ is taken for the investigated plasma conditions. This follows from Chen given that $\xi_p \equiv r/\lambda_D \approx 1\text{mm}/0.1\text{mm} \approx 10$ and $\Gamma \approx 0.607 + 2432\, e^{-7.01 \xi_p^{0.096}} \approx 1$.

In the right hand side of Eq. (3), a constant value is also taken for the electron temperature of the plasma, which will, as a result, be a source of uncertainty. Spatial and uncorrelated temporal[44] variations not accounted for will lead, respectively, to systematic and random errors on the final value of n (see Appendix A). Note that non-Maxwellian features of the electron energy distribution function (EEDF) such as a hotter population tail or some flow could also be potentially important, but comparison to sweeping bias Langmuir probe measurements indicated a limited disagreement to below ∼10%.

2. Plasma potential (V_p): Floating emissive probe

A DC heated, floating emissive probe made from a 0.1 mm diameter thoriated tungsten wire is used to measure the plasma potential, V_p. The probe is operated in the regime of strong thermionic electron emission, manifested itself as the saturation of the hot-probe floating potential with respect to the ground.[45] For the correct interpretation of this floating potential reading, the contribution from the heating voltage (V_h), typically $V_h \sim 4$ V, ought to be taken into consideration. Indeed, $1/2 V_h$ is subtracted from the measured voltage value.[46] In general, V_p is related to the corrected measured probe voltage, V_f^{hot}, by

$$V_p = V_f^{\text{hot}} + \alpha T_e, \tag{4}$$

where α is some constant $O(1)$ that depends on the particularities of the plasma under study.[47]

To assess how good an approximation $V_p \approx V_f^{\text{hot}}$ is, the smallness of the term αT_e in Eq. (4) was tested by comparing measurements to a sweeping Langmuir probe in the same discharge and at the same spatial location, using the second derivative of the measured IV traces to find the plasma potential[48,49] (see Appendix A).

3. Cross-field current ($j_{\perp,ExB}$): Two-probe method and rotating-wave approximation

The anomalous electron cross-field current resulting from fluctuations of local electric fields and plasma density is measured indirectly. For this measurement, the transport is assumed to be dominated by $E_\theta \times B$ variations, so that

$$j_{\perp,ExB}(r,\theta) = n(r,\theta) e \frac{E_\theta(r,\theta)}{B}. \tag{5}$$

The form of Eq. (5) suggests that, for a net radial electron transport (i.e., a nonvanishing azimuthal average) to exist, E_θ and n should have a small relative phase. In light of this, local measurements of density and azimuthal electric field are required. The two-probe method does so by using, simultaneously, an ion probe and an emissive probe, described in Subsections II C 1 and II C 2. These two distinct probes record n and V_p, respectively, from poloidally closely separated locations (a ∼ 0.3 cm apart) without significant shadowing.

In order to obtain E_θ from these measurements, the recorded V_p time series needs to be mapped onto the spatial domain, where the definition of $E_\theta \equiv -\nabla_\theta V_p$ may be applied. An approximated projection is possible under the assumption of what we call the "rotating wave approximation." This approximation scheme exploits the quasi-periodic rotation of the spoke, which is taken to be rigidly and uniformly whirling about the axis. In that case, the linear map is trivial, but gives rise to an uncertainty of up to ∼70% (see Appendix A). It is noted here that small turbulent scales are not resolved in this approach. The uncertainty does however not preclude the main conclusions in this paper. This will however be the dominant source of uncertainty in $j_{\perp,E\times B}$.

III. SPOKE CHARACTERISATION

A. Spoke activity reduction with metallic flange

The configuration in case II led to a clear reduction in spoke activity. This improvement in stability is described by a figure of merit defined as $\hat{V} = \frac{n - \langle n \rangle}{\langle n \rangle}$. That is to say, the relative size of the recorded density fluctuations is used as proxy for instability. An example of the reduced activity and the magnitudes for numerous B fields are shown in Fig. 3.

The density variations (see the right panel of Fig. 3) are reduced by a factor of ∼3.4(3) on average, over a range $B = 10$–150 G. This suggests that the stabilization mechanism introduced is not just incidental but holds for an extended set of parameters.

Nevertheless, the quieter plasma obtained with the metal does still show a prominent peak in its spectrum. The properties of this prevailing mode will now be compared to the spoke in case I.

B. Spoke changes due to the boundary

1. Changes in the shape and frequency

The most basic characteristics of a typical spoke in a Penning discharge are its slower frequency as compared to the $E \times B$ drift, its $m = 1$ mode nature and shape. The changes in these properties are exemplified in Fig. 4 and suggest that the spoke is of a different nature.

The shapes of the spokes in the top panels have been reconstructed based on data from simultaneous measurements of two ion probes, separated poloidally by an angle of $\pi/2$. The radial position of

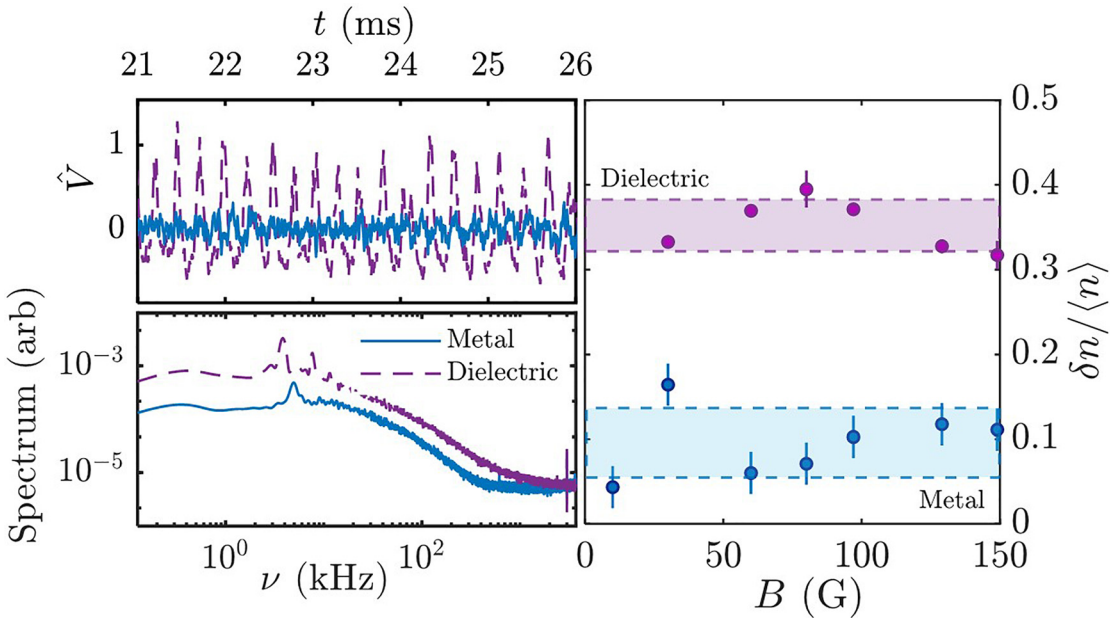

FIG. 3. Change in oscillatory behavior of the plasma when changing the boundary. (Left) Plots of normalized ion probe signal $\hat{V} = \frac{n-\langle n \rangle}{\langle n \rangle}$ for metal and glass boundaries, and their corresponding spectrum, for $B = 30$ G. (Right) Magnitude of variations, representative of instability, defined as $\delta n/\langle n \rangle$ as a function of B; δn is the standard deviation of the time signal of the main spectral component of the perturbation.

one of the probes was fixed at $r \sim 6$ cm, while the other changed so as to sample the radial extent of the spoke. The cross-correlation phase between the signals is the quantity shown in each of the polar plots, each arm within a diagram representing an opposite B direction.

These graphs show that the rotation in the $E \times B$ direction persists when the boundary is modified. However, an approximately 4-fold increase in the dispersion of the correlation phase in case II suggests that the spoke has lost coherency and/or rigidity. In addition, for case II, a significant loss of correlation at larger radii may be observed, reaching phase deviations of up to $\Delta\phi \sim \pi/2$ rad for the outermost locations. This observation may be linked to the spoke being located closer to the axis.

Regarding changes in the frequency of rotation (see lower panel), the modified oscillations occur approximately twice as fast, closer to the characteristic $E \times B$ drift frequency, which falls by a factor order ~2. As a way of example, for $B = 150$ G with the metal wall

$$\nu_{E\times B} = \frac{E_r}{2\pi r B} \approx \frac{50\mathrm{V m^{-1}}}{2\pi \times 4\mathrm{cm} \times 150\mathrm{G}} \approx 13\,\mathrm{kHz},$$

while for glass $\nu_{E\times B} \approx 43$ kHz. The corresponding spoke frequencies are 14 kHz and 6 kHz, respectively. The increased magnitude of ν is also accompanied by an increased complexity in $\nu(B)$, with the possibility of various competing modes, something to be considered in future work.

2. Changes in anomalous E × B electron cross-field current

The anomalous electron cross-field current, $j_{\perp,ExB}$, in the radial direction is investigated using the described two-probe method. Figure 5 shows the average magnitude of $j_{\perp,ExB}$ and classical transport values, as well as the relation of $j_{\perp,ExB}$ to the passage of the spoke. The figure also compares the measured cross field current with a cross field current estimate under the assumption that this is uniformly distributed in axial and azimuthal directions of the Penning discharge, i.e., $I_d/2\pi rL$.

The current distribution as a function of the spoke phase shows for case I (i.e., dielectric) a close relation between the $E \times B$ induced transport and the spoke. This correspondence appears as a narrow (i.e., FWHM of $\Delta\phi \sim \pi/4 - \pi/3$) conduction channel in Fig. 5. From the average profiles, it follows that this $E \times B$ current is the main contributor to the total discharge current; indeed, measurements lie within agreement (i.e., relative value of 40%–100%) with the uniform distribution estimates. These observations of $E \times B$ transport are consistent with the results from previous experiments performed in the same Penning discharge using a fast sweeping Langmuir probe[44] and Hall thrusters.[13,50]

In addition, $j_{\perp,ExB}$ is soundly anomalous, given that it lies around two orders of magnitude over the classical electron-neutral collisional transport levels [e.g., for $B = 30$ G and $r = 8$ cm, $j_{\mathrm{anom}}/j_{\mathrm{class}} \approx 90(70)$]. The classical transport may be estimated using experimentally measured field gradients in

$$j_r^{\mathrm{class}} = \frac{\sigma}{1 + (\omega_{ce}/\nu_{en})^2}\left(E_r + \frac{\partial T_e}{\partial r} + T_e \frac{\partial \ln n}{\partial r}\right), \qquad (6)$$

where

$$\sigma = \frac{ne^2}{m_e \nu_{en}}$$

and

$$\nu_{en} = n_0 \langle \sigma_{en} v \rangle,$$

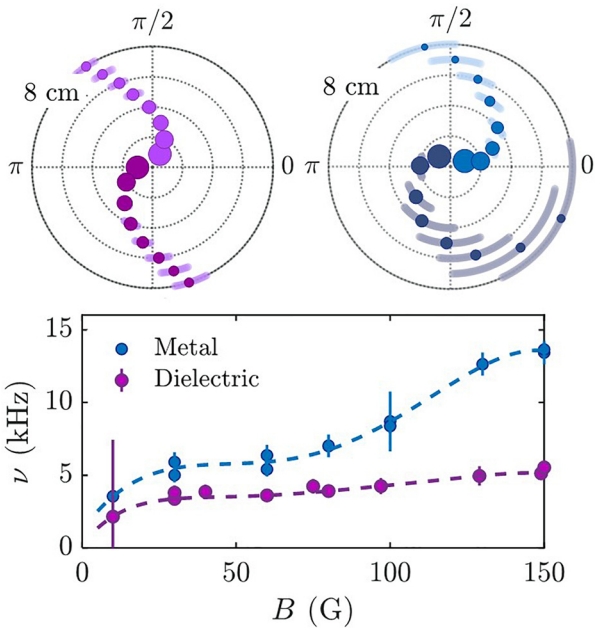

FIG. 4. (Lower) Rotation frequency $\nu = \nu(B)$ for metal and dielectric boundaries, showing the larger frequency in the metallic case. (Upper) Spoke shape for $B = 30$ G, each of the two arms in each plot corresponding to opposite directions of B. The size of the circles represents plasma density normalized to the central value. The shade represents the central 68% about the median. Comparing the shades at each radii of the lower arm in the right and left shapes, respectively, a roughly 4-fold difference is observed. Besides, the dispersion at $r = 8$ cm of the right arm is of the order of $\pi/2$. Differences in arm shapes and density amplitudes when the field is reversed lie within experimental uncertainty.

and $n_0 \approx 1.2 \times 10^{19}$ m^{-3} is the neutral density, ω_{ce} is the electron cyclotron frequency, σ_{en} is the electron-neutral collisional cross-section, and v is the speed of the electron species.

Importantly, it is here emphasized that the large scale spoke disturbances are seen to be the primary responsibilities for the majority of the transport (40%–100%). Given the magnitude of the classical contribution, the remaining of the transport could be associated with other processes mediated by a smaller scale.[36] This matter requires additional research to include measurements of smaller scale.

The large observed anomality may be also characterized by the effective Hall parameter defined as $\beta^i_{\text{eff}} = \omega_{ce}/\nu_{\text{eff}}$, where ν_{eff} is the effective collisional frequency that gives the observed current and i is a superscript that labels the two dielectric (D) and metal (M) cases. This nondimensional parameter is approximately $\beta^D_{\text{eff}} \approx 8(6)$ for $B = 30$ G in Case I at the edge $r = 8$ cm, consistent with the values presented in some numerical PIC simulations of Penning discharges.[33,36]

When the metallic flange is placed, the total cross field transport in the plasma drops very significantly (see Fig. 5), as expected from the short circuit effect. The anomalous character of transport, although still relevant, does also fall, as $j_{\perp,ExB}$ values are closer to classical collisional transport values [e.g., ∼6 times on average for $B = 30$ G cases, with $\beta^M_{\text{eff}} \approx 220(150)$]. At the same time, measured current is less correlated with the passage of the spoke; indeed, current profiles become spatially broader ($\Delta\phi \sim 2\pi/3$), noisier, and less prominent. This observation evidences the relation between transport and the spoke.

In conclusion, the reduction of the spoke activity appears connected to the drop in the total and anomalous cross field transports.

IV. COMPARISON WITH THEORY

The observed improvement in stability is now compared to the growth rate predictions of CSHI. To determine γ associated with the experimental conditions, mean time averaged radial profiles of V_p and n are measured empirically (see Appendix B). Taking $k_\theta \sim 1/r$, where r represents the radial position, all information needed for Eq. (2) is available. Figure 6 shows as scatter data the measured quantities in (E,L_n) space, for $B = 150$ G. Every pair of coordinates in this space is indeed associated with a growth rate, and this is represented as a colored contour.

According to CSHI theory, gradients are consistent with the improved stability; the gradients correspond to the dielectric case lying in a higher γ value. This prediction, though in qualitative agreement with experiment, presents a number of limitations that further theoretical work should amend.

To start with, it applies field gradient measurements from the nonlinear saturated regime to the linear theory formalism. It could be argued that, assuming that on average, due to the forcing and dissipation balance between the electron injection and the instability, the spoke should not change radial gradients dramatically, the qualitative linear description could be expected to be approximately correct. Perhaps more clearly, a failure of the linear treatment of CSHI is that it does not predict the observed prominence of the $m = 1$ mode; instead, it suggests that $m > 1$ are more unstable. In recent PIC simulations of the Penning discharge, the dominance of the m = 1 mode was also observed.[33,36] Such a preeminence of the lower modes is also commonplace in magnetrons ($m = 3$–5)[51] and annular Hall thrusters ($m = 2$–3),[11] and cylindrical Hall thrusters ($m = 1$).[13,18] Yet a definitive theoretical answer explaining the origin of such a nonlinear feature of the perturbations remains elusive and an open question to address.

Additional limitations of existing theories, especially when describing the metal case, come from disregarding several physically relevant features. For instance, due to the decrease in radial E, additional gradients (such as B or T_e) could gain relevance and need to be considered, e.g., using the more complete form of GDI.[24,28,29] Even with such an extension, relevant features of the system take us further away from classical CSHI: axial uniformity may break down (there is a significant net axial current flow), the short circuit effect[37] is not accounted for, and possibly significant sheaths[30,52] may be present. A more detailed numerical, theoretical, and experimental exploration is left for future work.

Nonetheless, the qualitatively consistent behavior with the electric field and density gradient trends following from CSHI suggest as a possible theoretical framework the more general GDI theory, perhaps including additional effects such as the sheath.

V. CONCLUSION

The spoke instability sustained in a low-density plasma in an $E \times B$ Penning discharge has been demonstrated to be significantly reduced by changing boundary properties. The introduction of an all-metallic surface connected to the anode in front of the flow of electrons from the cathode led to a reduction in the prominence of fluctuations, as hypothesized. However, a modified saturated structure

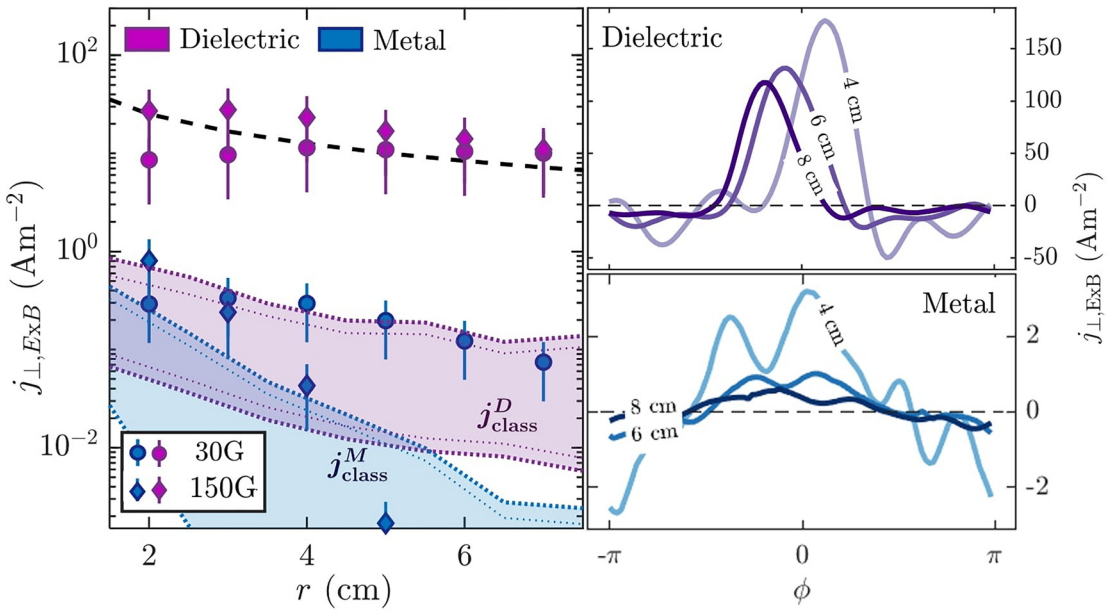

FIG. 5. (Left) Comparison of time averaged cross field anomalous current density with the radius for metal and glass boundaries, shown for $B = 30$, 150 G. The shaded regions represent classical transport estimates given measured gradients for values of B spanning 30–150 G. The broken black curve corresponds to a uniform distribution of I_d, i.e., $j = I_d/2\pi rL$. (Right) Spoke phase resolved transport at different radii ($r = 4$, 6, 8 cm), with $\phi = 0$ corresponding to the density maximum ($B = 30$ G).

persisted, characterized by a faster, more radially confined and less coherent rotation than that of the spoke with the dielectric.

The cross field anomalous $E \times B$ electron transport due to the large-scale spoke perturbations was measured *in-situ* and, for the dielectric, seen to account for 40%–100% of the total discharge current, resulting in $\beta^D_{\text{eff}} \approx 10$ consistent with computational work.[33,36] Transport becomes more spread and closer to levels of classical collisional transport with the metal as the boundary ($\beta^M_{\text{eff}} \approx 10\beta^D_{\text{eff}}$). These changes in transport imply an inhibited radial loss of electrons, which could be of relevance in design of devices such as Hall Thrusters (more specifically, anode layer Hall thruster, Camila Hall thruster,[53,54] segmented Hall thruster,[55,56] and magnetically shielded Hall thruster[57]) and sputtering magnetrons.[14,51]

Finally, the observations were shown to be generally consistent with the electric field and density gradient trends following from the standard collisionless Simon-Hoh instability. However, several aspects such as the dominance of low m-modes remain unexplained. Moreover, additional gradients,[24,28,29] sheath effects,[30,52] or significant axial nonuniformities are recognized as likely relevant aspects, especially in the metallic case, and should be considered in a more comprehensive framework. The investigation of these added complexities is left for future numerical, experimental, and theoretical work.

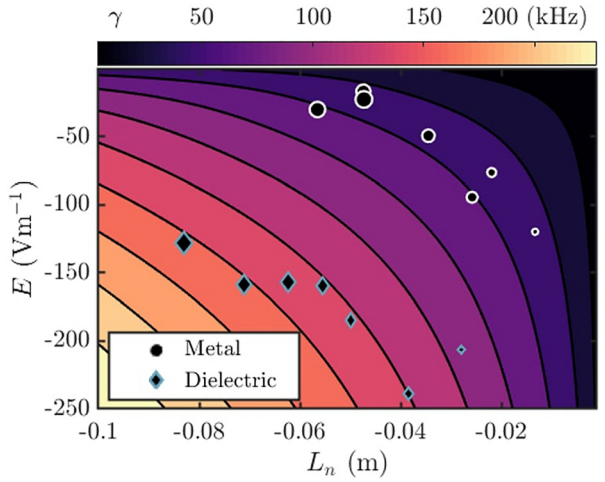

FIG. 6. Collisionless Simon-Hoh instability growth rate, γ, in $E - L_n$ parameter space. The scattered data represent mean measured gradients for $B = 150$ G, with the increasing symbol size representing larger radii measurements for 1–8 cm.

ACKNOWLEDGMENTS

Thanks to Brian Kraus, Andy Alt, and Johan Carlsson for fruitful discussions.

This work was supported by the Air Force Office of Scientific Research (AFOSR).

APPENDIX A: EXPERIMENTAL UNCERTAINTY

In this appendix, the uncertainty sources taken into consideration for the measurements in this paper are spelled out for completeness.

1. Plasma density (n)

See Table I for the uncertainty contribution to the plasma density n measurement with ion probes. The first two entries (measured radial variation in temperature $T_e(r)$ based on floating cold

TABLE I. Uncertainty sources to the plasma density n: radial variation in temperature $T_e(r)$, calculated correction parameter[43] $\Gamma(r)$, time fluctuations[44] of $T_e(t)$, theoretical indeterminacy[58] in temperature measurement (ΔT_{TH}), and correction for sheath expansion (Δn_{SAT}). The total uncertainty results from the statistical combination of all.

Source	$\Delta n/n$ (%)
$\Gamma(r)$	15
$T_e(r)$	25
$T_e(t)$	5
ΔT_{TH}	10
Δn_{SAT}	10
Δn_{TOT}	20

and emissive probe[45] and calculated correction parameter[43] $\Gamma(r)$) are anticorrelated and result from disregarding spatial variations. The remaining represent uncorrelated sources such as time fluctuations[44] of $T_e(t)$, theoretical indeterminacy[58] in the temperature measurement (ΔT_{TH}), and correction for sheath expansion from the measured saturation current changes with bias voltage (Δn_{SAT}). The total uncertainty is obtained by combining all these various sources of indeterminacy.

2. Plasma potential (V_p)

See Table II for the uncertainty contribution to the plasma potential V_p measurement with the emissive probe. The first entry corresponds to the error due to ignoring the term αT_e in Eq. (4), which is found to be $-\alpha \sim 0.1$–0.2 and $T_e \sim 2$ eV. This itself has a randomly fluctuating part[44] to it ~5%. The uncertainty in the heating voltage V_h measurement also contributes, even assuming the theoretical correctness of the $1/2V_h$ correction.[46]

3. Electron cross-field current ($j_{\perp,ExB}$)

See Table III for the uncertainty contribution to the electron cross-field current $j_{\perp,ExB}$ measurement with the two-probe method. The first two entries correspond to the error in determining E_θ: due to fluctuations in αT_e that modify the actual V_p and local variations in the rotation speed ω_{rot}, whose uniformity was assumed in the rotating wave approximation. The ω_{rot} variations are assessed experimentally using correlation of signals from two closely separated identical ion probes. Related to n, an overall scaling uncertainty Δn is to be considered. Also, some error arises due to noncoincident measurements of n and E_θ; this is estimated considering a displacement assuming a sinusoidal $n(\theta)$ profile.

TABLE II. Uncertainty sources to the plasma potential V_p, from ignoring the term αT_e in Eq. (4), and the heating voltage V_h.

Source	ΔV_p (V)
αT_e	0.2–0.4
V_h	0.1
$\Delta V_{p,TOT}$	0.2–0.4

TABLE III. Uncertainty contribution to the electron cross-field current $j_{\perp,ExB}$: fluctuations in αT_e, local variations in rotation speed ω_{rot}, overall scaling uncertainty Δn, and noncoincident ($\Delta\theta$) measurements of n and E_θ.

Variable affected	Source	$\Delta j/j$ (%)
E_θ	$\Delta(\alpha T_e)$	1
	ω_{rot}	70
n	Δn	20
	$n(\Delta\theta)$	5
Δj_{tot}	…	70

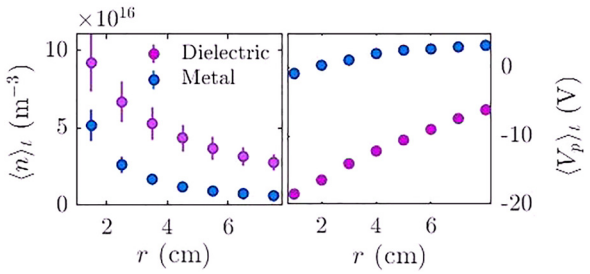

FIG. 7. Density and plasma potential profiles for $B = 150$ G for both metallic and dielectric boundary cases.

APPENDIX B: FIELD GRADIENT SAMPLE

An example of what the field distribution looks like is here presented in Fig. 7 for both cases I and II for $B = 150$ G.

REFERENCES

[1] A. I. Morozov, "The conceptual development of stationary plasma thrusters," Plasma Phys. Rep. **29**, 235 (2003).
[2] J. P. Boeuf, "Tutorial: Physics and modeling of hall thrusters," J. Appl. Phys. **121**, 011101 (2017).
[3] D. M. Goebel and I. Katz, *Fundamentals of Electric Propulsion: Ion and Hall Thrusters* (Wiley, New York, 2008).
[4] I. Levchenko, S. Xu, G. Teel, D. Mariotti, M. Walker, and M. Keidar, "Recent progress and perspectives of space electric propulsion systems based on smart nanomaterials," Nat. Commun. **9**, 879 (2018).
[5] S. Swann, "Magnetron sputtering," Phys. Technol. **19**(2), 67 (1988).
[6] P. Kelly and R. Arnell, "Magnetron sputtering: A review of recent developments and applications," Vacuum **56**, 159–172 (2000).
[7] P. F. Carcia, R. S. McLean, M. H. Reilly, and G. J. Nunes, "Transparent zno thin-film transistor fabricated by rf magnetron sputtering," Appl. Phys. Lett. **82**, 1117 (2003).
[8] V. V. Zhurin, H. R. Kaufman, and R. S. Robinson, "Physics of closed drift thrusters," Plasma Sources Sci. Technol. **8**, R1 (1999).
[9] A. Lazurenko, V. Krasnoselskikh, and A. Bouchoule, "Experimental insights into high-frequency instabilities and related anomalous electron transport in hall thrusters," IEEE Trans. Plasma Sci. **36**, 1977 (2008).
[10] E. C. S. Megaw, "Magnetron oscillations," Nature **134**, 324–325 (1934).
[11] M. S. McDonald and A. Gallimore, "Rotating spoke instabilities in Hall thrusters," IEEE Trans. Plasma Sci. **39**, 2952 (2011).
[12] D. Liu, R. E. Huffman, R. D. Branam, and W. A. Hargus, "Ultrahigh speed images of Hall thruster azimuthal instabilities," IEEE Trans. Plasma Sci. **42**, 2656 (2014).
[13] C. L. Ellison, Y. Raitses, and N. J. Fisch, "Cross-field electron transport induced by a rotating spoke in a cylindrical hall thruster," Phys. Plasmas **19**, 013503 (2012).

[14]A. Anders and Y. Yang, "Direct observation of spoke evolution in magnetron sputtering," Appl. Phys. Lett. **111**, 064103 (2017).
[15]A. P. Ehiasarian, A. Hecimovic, T. de los Arcos, R. New, V. S. von der Gathen, M. Boke, and J. Winter, "High power impulse magnetron sputtering discharges: Instabilities and plasma self-organization," Appl. Phys. Lett. **100**, 114101 (2012).
[16]K. I. Thomassen, "Turbulent diffusion in a penning-type discharge," Phys. Fluids **9**, 1836 (1966).
[17]G. S. Janes and R. S. Lowder, "Anomalous electron diffusion and ion acceleration in a low-density plasma," Phys. Fluids **9**, 1115 (1966).
[18]J. B. Parker, Y. Raitses, and N. J. Fisch, "Transition in electron transport in a cylindrical hall thruster," Appl. Phys. Lett. **97**, 091501 (2010).
[19]P. Poolcharuansin, F. L. Estrin, and J. W. Bradley, "The use of segmented cathodes to determine the spoke current density distribution in high power impulse magnetron sputtering plasmas," J. Appl. Phys. **117**, 163304 (2015).
[20]G. Janes, J. Dotson, and T. Wilson, "Electrostatic acceleration of neutral plasmas - momentum transfer through magnetic fields," Technical Report No. NP-12154, Avco Corporation, Avco-Everett Research Laboratory, Everett, MA (1962).
[21]A. B. Mikhailovskii, *Electromagnetic Instabilities in an Inhomogeneous Plasma* (IoP, Bristol, Philadelphia, New York, 1991).
[22]M. Dobrowolny, "Effect of non-uniform electric fields on drift instabilities," Plasma Phys. **12**, 463 (1970).
[23]A. A. Litvak and N. J. Fisch, "Rayleigh instability in hall thrusters," Phys. Plasmas **11**, 1379 (2004).
[24]A. I. Smolyakov, O. Chapurin, W. Frias, O. Koshkarov, I. Romadanov, T. Tang, M. Umansky, Y. Raitses, I. D. Kaganovich, and V. P. Lakhin, "Fluid theory and simulations of instabilities, turbulent transport and coherent structures in partially-magnetized plasmas of E × B discharges," Plasma Phys. Controlled Fusion **59**, 014041 (2017).
[25]Y. Sakawa, C. Josh, P. K. Kaw, F. F. Chen, and V. K. Jain, "Excitation of the modified Simon-hoh instability in an electron beam produced plasma," Phys. Fluids B: Plasma Phys. **5**, 1681 (1993).
[26]A. Simon, "Instability of a partially ionized plasma in crossed electric and magnetic fields," Phys. Fluids **6**, 382 (1963).
[27]F. C. Hoh, "Instability of penning-type discharges," Phys. Fluids **6**, 1184 (1963).
[28]W. Frias, A. I. Smolyakov, I. D. Kaganovich, and Y. Raitses, "Long wavelength gradient drift instability in hall plasma devices. i. Fluid theory," Phys. Plasmas **19**, 072112 (2012).
[29]W. Frias, A. I. Smolyakov, I. D. Kaganovich, and Y. Raitses, "Long wavelength gradient drift instability in hall plasma devices. ii. Applications," Phys. Plasmas **20**, 052108 (2013).
[30]V. Morin and A. I. Smolyakov, "Modification of the Simon-Hoh instability by the sheath effects in partially magnetized E × B plasmas," Phys. Plasmas **25**, 084505 (2018).
[31]J.-P. Boeuf and B. Chaudhury, "Rotating instability in low-temperature magnetized plasmas," Phys. Rev. Lett. **111**(15), 155005 (2013).
[32]J.-P. Boeuf, "Rotating structures in low temperature magnetized plasmas-insight from particle simulations," Front. Phys. **2**, 74 (2014).
[33]J. Carlsson, I. Kaganovich, A. Powis, Y. Raitses, I. Romadanov, and A. Smolyakov, "Particle-in-cell simulations of anomalous transport in a penning discharge," Phys. Plasmas **25**, 061201 (2018).
[34]F. Taccogna and P. Minelli, "Three-dimensional fully kinetic particle-in-cell model of hall-effect thruster," in International Electric Propulsion Conference (2011).
[35]K. Matyash and R. Schneider, "Particle in cell simulation of plasma thrusters," in 19th IEEE Pulsed Power Conference (PPC) (2013).
[36]A. T. Powis, J. A. Carlsson, I. D. Kaganovich, Y. Raitses, and A. Smolyakov, "Scaling of spoke rotation frequency within a penning discharge," Phys. Plasmas **25**, 072110 (2018).
[37]A. Simon, "Ambipolar diffusion in a magnetic field," Phys. Rev. **98**, 317–318 (1955).
[38]Y. Raitses, I. Kaganovich, and A. Smolyakov, "Effects of the gas pressure on low frequency oscillations in exb discharges," in Proceedings on Joint Conference 30th ISTS, 34th IEPC, and 6th NSAT (2015).
[39]B. M. Annaratone, A. Escarguel, T. Lefevre, C. Rebont, N. Claire, and F. Doveil, "Rotation of a magnetized plasma," Phys. Plasmas **18**, 032108 (2011).
[40]W. Gekelman, H. Pfister, Z. Lucky, J. Bamber, D. Leneman, and J. Maggsl, "Design, construction, and properties of the large plasma research device the LAPD at UCLA," Rev. Sci. Instrum. **62**, 2875 (1991).
[41]Y. Raitses, J. K. Hendryx, and N. J. Fisch, "A parametric study of electron extraction from a low frequency inductively coupled rf-plasma source," in *The 31st International Electric Propulsion Conference* (2009), Paper No. IEPC-2009-024.
[42]R. L. Merlino, "Understanding Langmuir probe current-voltage characteristics," Am. J. Phys. **75**(12), 1078–1085 (2007).
[43]F. F. Chen, J. D. Evans, and D. Arnush, "A floating potential method for measuring ion density," Phys. Plasmas **9**(4), 1449–1455 (2002).
[44]V. Skoutnev, P. Dourbal, E. Rodrguez, and Y. Raitses, "Fast sweeping probe system for characterization of spokes in e b discharges," Rev. Sci. Instrum. **89**, 123501 (2018).
[45]J. Sheehan, Y. Raitses, N. Hershkowitz, and M. McDonald, "Recommended practice for use of emissive probes in electric propulsion testing," J. Propul. Power **33**, B35697 (2017).
[46]E. Mravlag and P. Krumm, "Space potential measurements with a continuously emitting probe," Rev. Sci. Instrum. **61**, 2164 (1990).
[47]B. F. Kraus and Y. Raitses, "Floating potential of emitting surfaces in plasmas with respect to the space potential," Phys. Plasmas **25**(3), 030701 (2018).
[48]V. A. Godyak and V. I. Demidov, "Probe measurements of electron-energy distributions in plasmas: what can we measure and how can we achieve reliable results?," J. Phys. D: Appl. Phys. **44**, 269501 (2011).
[49]M. J. Druyvesteyn and F. M. Penning, "The mechanism of electrical discharges in gases of low pressure," Rev. Mod. Phys. **12**, 87 (1940).
[50]M. Mcdonald, C. Bellant, B. S. Pierre, and A. Gallimore, "Fast sweeping probe system for characterization of spokes in e b discharges," in *47th AIAA/ASME/SAE/ASEE Joint Propulsion Conference and Exhibit* (AIAA, 2011).
[51]T. Ito, C. V. Young, and M. A. Cappelli, "Self-organization in planar magnetron microdischarge plasmas," Appl. Phys. Lett. **106**, 254104 (2015).
[52]A. I. Smolyakov, W. Frias, I. D. Kaganovich, and Y. Raitses, "Sheath-induced instabilities in plasmas with E0 x B-0 drift," Phys. Rev. Lett. **111**, 115002 (2013).
[53]I. Kronhaus, A. Kapulkin, V. Balabanov, M. Rubanovich, M. Guelman, and B. Natan, "Investigation of physical processes in CAMILA hall thruster using electrical probes," J. Phys. D: Appl. Phys. **45**, 175203 (2012).
[54]A. Kapulkin, V. Balabanov, M. Rubanovich, E. Behar, L. Rabinovich, and A. Warshavsky, "Camila hall thruster new results," in *32nd International Electric Propulsion Conference* (IEPC, 2011).
[55]N. J. Fisch, Y. Raitses, L. A. Dorf, and A. A. Litvak, "Variable operation of hall thruster with multiple segmented electrodes," J. Appl. Phys. **89**, 2040 (2001).
[56]K. D. Diamant, J. E. Pollard, R. B. Cohen, Y. Raitses, and N. J. Fisch, "Segmented electrode Hall thruster," J. Propul. Power **22**, 1396 (2006).
[57]R. W. Conversano, D. M. Goebel, I. G. Mikellides, R. R. Hofer, and R. E. Wirz, "Performance analysis of a low-power magnetically shielded Hall thruster: Computational modeling," J. Propul. Power **33**(4) (2017).
[58]Y. Raitses, D. Staack, A. Smirnov, and N. J. Fisch, "Space charge saturated sheath regime and electron temperature saturation in hall thrusters," Phys. Plasmas **12**, 073507 (2005).